Determination of internal-target thickness and experimental luminosity from beam energy loss at HIRFL-CSRe*

Cao-Jie Shao(邵曹杰)[1,2,3;1)] De-Yang Yu(于得洋)[1] Rong-Chun Lu(卢荣春)[1] Tie-Cheng Zhao(赵铁成)[1]
Rui-Shi Mao(毛瑞士)[1] Jie Li(李杰)[1] Ying-Li Xue(薛迎利)[1] Wei Wang(王伟)[1] Bian Yang(杨变)[1]
Ming-Wu Zhang(张明武)[1] Jun-Liang Liu(刘俊亮)[1,3] Zhang-Yong Song(宋张勇)[1]
Xiao-Hong Cai(蔡晓红)[1] Xi-Meng Chen(陈熙萌)[2] Da-Yu Yin(殷达钰)[1] Li-Jun Mao(冒立军)[1]
Xiao-Dong Yang(杨晓东)[1] Jian-Cheng Yang(杨建成)[1] You-Jin Yuan(原有进)[1]

[1] Institute of Modern Physics, Chinese Academy of Sciences, Chinese Academy of Sciences，Lanzhou 730000, China
[2] School of Nuclear Science and Technology, Lanzhou University, Lanzhou 730000, China
[3] University of Chinese Academy of Sciences, Beijing 100049, China

Abstract: The target thickness for nitrogen was determined from the beam energy loss in HIRFL-CSRe during the experimental study of the K-REC process in 197 MeV/u Xe^{54+}-N_2 collisions. Furthermore, the corresponding integrated luminosity of $(1.15\pm0.06)\times10^{30}$ cm^{-2} was obtained. As an independent check on the energy-loss method, we have also determined the integrated luminosity by measuring the produced X-rays from the K-REC process with a known differential cross section. The values of $(1.12\pm0.06)\times10^{30}$ and $(1.09\pm0.06)\times10^{30}$ cm^{-2} were obtained by using two high-purity germanium (HPGe) detectors which were oriented at 90° and 120° with respect to the beam path, respectively. The consistent results confirmed the feasibility of the energy-loss method, which may have an important impact on future internal target experiments at HIRFL-CSRe.

Keywords: heavy-ion storage ring, internal target, luminosity, target thickness, energy loss

PACS: 29.20.db, 29.25.Pj, 34.50.Bw **DOI:** 10.1088/1674-1137/40/11/117002

1 Introduction

Internal target facilities have been widely used at storage rings for experimental studies in the fields of atomic, nuclear and particle physics, because the storage-ring operation with the combination of internal targets and cooling of the stored beams allows high-precision experiments to be made with high luminosities and low physics background [1, 2]. The HIRFL-CSR has been in operation since 2008 and can provide all ion species from protons to uranium, with energy variable from ion source energy to 1 GeV/u ($A/q=2$) [3, 4]. An internal target facility, dedicated to ion-atom collision experiments, was constructed at one straight section of CSRe [5, 6]. It can provide atom beams of 10^{11}—10^{13} atoms/cm^2 for inert gases and small molecular gases (e.g. CH_4) under ultra-high vacuum (UHV) background, usually 10^{-9} Pa, for experiments.

Experiments with an internal target at a storage ring have many advantages. However, it is difficult to determine the absolute cross section of a reaction where luminosity cannot be simply established through macroscopic measurements. The luminosity of an internal target experiment can usually be given by

$$L=n_{\rm ion}D_{\rm T}f, \tag{1}$$

where $n_{\rm ion}$ is the number of circulating ions, $D_{\rm T}$ the target areal density, and f the revolution frequency of the stored ions. In an ideal scattering experiment with an internal target, the profile of the coasting beam should be far less than that of the target beam, and the center of the beam and target coincide perfectly, therefore the target thickness can be determined by multiplying the target volume density and the path of the beam in the target d, which was approximately 3.6 mm in our case, as shown in Fig. 1. The target volume density can be derived with pressure difference measurements which are calibrated by the flow rate of atomic beam [7]. If so, the luminosity can be determined by measuring the number and revolution frequency of the ions in the storage ring, which can be done accurately by a DC current transformer (DCCT) and Schottky pick-up device [8], respectively.

Received 12 April

∗ Supported by National Natural Science Foundation of China (11179017, 11105201, U1532130, and U1332206)

1) E-mail: c.shao@impcas.ac.cn

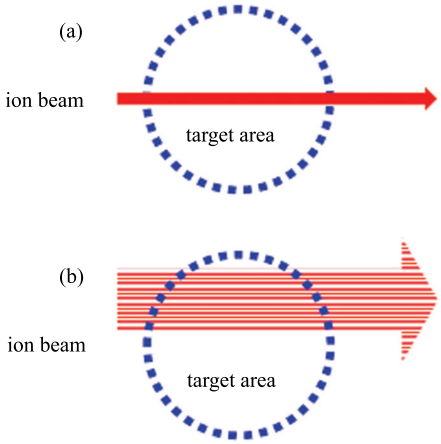

Fig. 1. (color online) Schematic views of (a) ideal and (b) possible beam-target overlap.

Unfortunately, at the specific condition of experiments with internal cluster-jet target at CSRe, such measurements are known to be imprecise due to the following several factors. Firstly, the distribution of volume density of a cluster jet target is usually represented as a homogeneous cylinder with a uniform value along the path of the beam in the target. This simple model was recently proved inappropriate for the actual density distribution [9]. Secondly, the profile of the cooled beam may be comparable to the size of the target beam. In such a case, the target thickness cannot be obtained by simply multiplying the target volume density and the path of the beam in the target. Instead, one has to consider the particular intensity distribution of the beam at the point of collision. Finally, it is very challenging to ensure that the beam and the target center coincide perfectly during the whole experiment. Therefore, in order to measure the effective target thickness accurately, one has to monitor the intensity distributions of the ions and target and the relative position between them in real time. Up to now, it has not been feasible to monitor all these parameters instantaneously in our experiments.

Here we present the first experimental determination of the effective target thickness from the beam energy losses at the internal target in HIRFL-CSRe. The energy-loss technique were developed by H. J. Stein et al. to determine a hydrogen cluster-jet target at the COSY-Jülich accelerator with an proton beam of energy 2.65 GeV [10]. It is simple in principle and independent of the profiles of the targets beam and beams. The repeated passages of a coasting ion beam through a thin target in a storage ring will induce a shift of revolution frequency due to energy loss in the target. Since the revolution-frequency shift rate is proportional to the target thickness and the beam-target overlap, its measurement offers the possibility to determine the effective target thickness and hence the corresponding luminosity in an experiment. The measurements here are expected to provide the accurate target thickness and luminosity for the absolute cross-section study on future internal target experiments, and also provide some reference values for the study of the beam loss mechanism of heavy ions at HIRFL-CSRe.

2 Determination of target thickness from beam energy loss

The experiment was carried out at CSRe, which is equipped with an electron cooling system (electron-cooler) [11] and an internal cluster-jet target. The experiment was carried out with the stored coasting beams of bare Xenon ions ($^{131}Xe^{54+}$) with an intensity of about $(3\sim8)\times10^6$ and a kinetic energy of 197 MeV/u. CSRe has three typical operation modes, i.e., internal target mode, normal mode and isochronous mode. In the present case, the internal target mode with the transition gamma $\gamma_{tr}=2.457$ was imposed [3], where the ion beam was most focused at the target region to maximize the beam-target overlap. The electron-cooler was used for increase of the phase space density of the injected beam and hence provided a high quality, dense stored beam for in-ring experiments.

In the internal target section, the beam crossed with a N_2 cluster jet, which was produced by a four-stage differential pumping system with its nozzle cooled to about 90 K. The jet had a intensity profile with a diameter of about 3.6 mm at the interaction zone. A chopper at the second stage of the cluster source was used to control whether or not to allow the target beam into the collision chamber. It takes less than a second to turn the target beam on or off using the chopper. The target density was stable during the whole experiment, and the background vacuum was better than 3×10^{-9} Pa. To optimize the beam-target overlap, a photomultiplier tube (PMT) was employed behind a quartz window of the collision chamber to count the visible and ultraviolet photons, which were emitted when the ions passed through the internal target. Without the ion beam, the counting rate of the PMT was typically less than 10 Hz, while with the optimized beam-target overlap the counting rate ranged from 600 to 2500 Hz. By locally shifting its orbit and monitoring the counting rate of the PMT, the beam was able to overlap with the cooling electron beam and cross with the internal target jet simultaneously.

The ion beam that had been injected into the CSRe was first cooled before the N_2 target beam was turned on. Then the electron-cooler was turned off while the target beam was turned on (this defines the origin of time $t=0$ s), resulting in a shift in the revolution frequency due to the energy loss. The revolution-frequency spectrum of the circulating ions was measured by CSRe Schottky-

pickup diagnostics. The typical longitudinal Schottky power spectrum for the 6th harmonic of the revolution frequency is shown in Fig. 2. The measurement was started at about $t = 50$ s and lasted over a period of 40 s. It can be seen obviously from the right side of the figure that the center of the spectrum shifts to the lower frequencies.

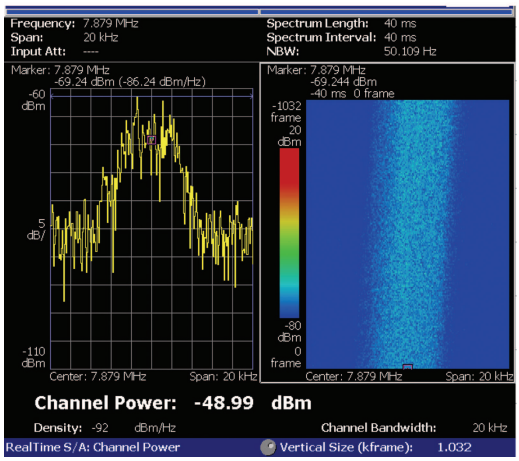

Fig. 2. (color online) The longitudinal Schottky power spectra recorded within about 40 s during the blow up measurement with the electron-cooler off. The measurement was done for the 6th harmonic of the revolution frequency and started after 50 s when the electron-cooler was turned off.

The effective target thickness can be determined from the frequency-shift rate according to [10]

$$D_f = \frac{1+\gamma}{\gamma}\frac{1}{\eta}\frac{1}{(\mathrm{d}E/\mathrm{d}x)m}\frac{T_0}{f_0^2}\frac{\mathrm{d}f}{\mathrm{d}t}, \tag{2}$$

where γ is the Lorentz factor, $\eta = \gamma_0^{-2} - \gamma_{\mathrm{tr}}^{-2}$ the frequency dispersion function [12], $\mathrm{d}E/\mathrm{d}x$ the stopping power of the ions in the target, m the mass of the target atom, and $T_0 = (\gamma - 1)\mathrm{mc}^2$ the beam kinetic energy. Here γ, and T_0 are determined by the measured revolution frequency and nominal circumference of the accelerator, and $\mathrm{d}E/\mathrm{d}x$ is calculated from the Bethe-Bloch formula as is done in Ref. [13]. The revolution-frequency shift Δf is determined by analyzing the Schottky noise spectrum of the coasting Xe^{54+} beam. The revolution-frequency distribution is characterized by a mean revolution frequency f_0, which is directly related to the longitudinal ion momentum.

3 Results and discussion

3.1 Results of target thickness

Figure 3 shows a typical result for the Schottky power spectra obtained during about 500 s cycles after the electron-cooler was switched off and the target was turned on ($t = 0$). Due to the momentum spread of the coasting beam, the spectra have broadening widths. The center of the spectrum shifted to the lower frequency due to the energy loss and the width of the distribution increased due to energy straggling. The overall revolution-frequency shift in the cycle is negative because at 197 MeV/u the accelerator is working under the transition point.

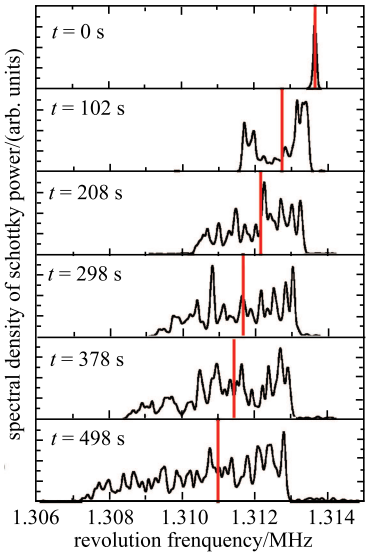

Fig. 3. (color online) Schottky power spectra obtained during a 500 s cycle. The measurement was started after the ion beam in CSRe was cooling down to a momentum spread $\Delta p/p$ of 2.2×10^{-5} ($t = 0$ s). The mean revolution frequencies indicated by vertical lines decreases through the cycle.

Because the spectrum analyzer measures primarily the Schottky noise power, which is proportional to the number of particles N in the ring, the mean value of revolution-frequency distribution can be evaluated directly by following formula

$$f_{\mathrm{mean}} = \frac{\int_{-\infty}^{\infty} I(f) f \mathrm{d}f}{\int_{-\infty}^{\infty} I(f) \mathrm{d}f} \tag{3}$$

and it is labeled by the vertical lines in Fig. 3.

The time dependence of the mean revolution-frequency shift Δf is shown for a typical cycle in Fig. 4. The fitting result by the least square is shown as the solid line and is well described by a second order polynomial:

$$\Delta f = 0.005471t^2 - 7.717t - 76.46, \tag{4}$$

where the units of t and Δf are second and Hz, respectively. Hence the rate of revolution-frequency shift can

be given by $\mathrm{d}f/\mathrm{d}t = (0.0109t - 7.717)$ Hz/s. This result means that rate of revolution-frequency shift changes a little during testing since the overlap of beam-target changes and beam profile changes due to the emittance growth over the cycle.

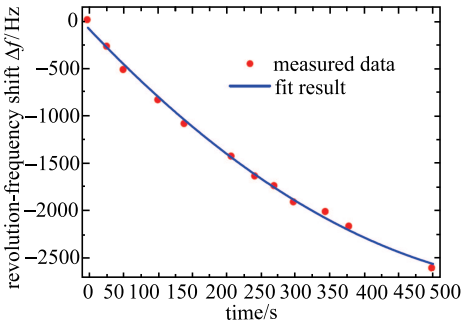

Fig. 4. (color online) Typical mean revolution-frequency shift derived from Schottky power spectra of the type illustrated in Fig. 3. This results show revolution-frequency shift decrease with a slope $\mathrm{d}f/\mathrm{d}t = 7.717 \pm 0.025$ Hz/s at the beginning of the measurement and then slow down to 3.27 ± 0.011 Hz/s at the ending of measurement.

Using Eq. (2) a first approximation to the value of the effective target thickness can now be given, assuming that the measured revolution-frequency shift was dominantly caused by the target itself. A stopping power of 7845 MeVcm^{2}g^{-1} for Xe^{54+} in a nitrogen target is adopted. The result for the particular machine cycle, which is typical for the whole run, is $D_{\mathrm{T}} = 2.26 \times 10^{12}$ atoms/cm^2 at the beginning of the measurement and then decreases to 9.6×10^{11} atoms/cm^2 at the ending (about $t = 400$ s) of measurement. This result contains, of course, a contribution arising from the residual gas in the ring. The systematic correction is needed to take account of this.

The contribution of the residual gas in the ring to the energy loss was measured with the target switched off (Fig. 5). The resulting revolution-frequency shift rate was $\mathrm{d}f/\mathrm{d}t = 0.168 \pm 0.005$ Hz/s, which corresponds to a 3% effect as compared to that obtained with the target. The energy loss caused by the nitrogen not being localized in the target beam is neglected here due to the vacuum of 9.0×10^{-10} and 1.1×10^{-9} Pa being obtained in the scattering chamber without and with gas in, and these values are much better than the mean value of 5.0×10^{-9} Pa in CSRe. Therefore, the effective thickness of 2.21×10^{12} atoms/cm^2 were determined at the beginning of measurement and then decreased to 9.06×10^{11} atoms/cm^2 at the end of the measurement.

However, the value of target thickness estimated by the pressure difference measurements, which were calibrated by the flow rate of atomic beam [7], is 3.52×10^{12} atoms/cm^2. It was larger by a factor of 1.6 than the corresponding thickness determined from the beam energy loss. Therefore, the beam-target overlap is incomplete in this experiment and the overlap factor between the beam and cluster-jet is estimated to be about 60% and decreases over time. The effective target thickness might also decrease due to the emittance growth or the dispersion not being zero, and this would induce a slight nonlinear time dependence of the revolution-frequency shift. Because of the dispersion $D_x \approx 0$ at the target position, the ion beam should not move away from the target when its energy decreases. The beam can also experience emittance growth through multiple small angle Coulomb scattering in the target. At each target traversal the emittance of the ion beam increases slightly in both transverse directions, leading to larger beam profiles, and as a consequence, the beam-target overlap may be reduced.

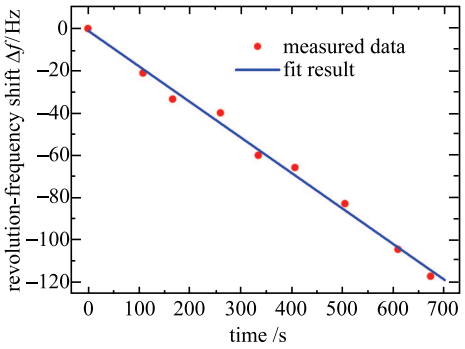

Fig. 5. (color online) Typical mean revolution-frequency shift owing to the residual gas derived from the Schottky power spectra. The resulting revolution-frequency shift rate was $\mathrm{d}f/\mathrm{d}t = 0.168 \pm 0.005$ Hz/s.

Figure 6 shows the counting rate of the PMT divided by the beam current in one of the cycles under different cooler conditions. The open circles represent the test results while electron cooling device was kept on during the whole cycle. As the counting rate of the PMT is proportional both to the Xe^{54+} beam intensity and to the effective target thickness, it could be used as an indicator of the beam-target overlap factor, supposing the beam intensity and target thickness are unchanged during the measurement. From the figure one can see that the overlap of the beam and target are nearly constant. However, the beam-target overlap decreased obviously if the electron-cooler was turned off after the beam was cooled down, as indicated by the open squares in Fig. 6. So the electron-cooler plays an extremely important role in experiments with an internal target at storage rings. It can not only diminish the effects of Doppler broadening by reducing the longitudinal momentum dispersion of the beam [14], but also improves the experimental luminosity obviously by enhancing the overlap factor of the beam and target.

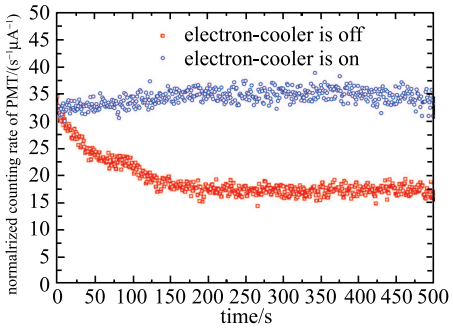

Fig. 6. (color online) The counting rates of PMT normalized by beam current under different cooler conditions. The open circles represent the test results while electron-cooler was kept on during the whole cycle. The open squares represents the result while electron-cooler was turned off after the beam was cooled down.

3.2 Results of luminosity

Figure 7(a) shows the number of Xe^{54+} ions $n_{\rm ion}$ in CSRe for successive cycles. Within each cycle the ion number decreases with time due to beam losses from interactions with the internal target and electron beam in the electron-cooler mainly by the radiative electron recombination (REC) process [14]. This is unlike the case of the proton beam where the REC process is almost impossible. In addition, the initial beam current also varies from cycle to cycle, so the mean number of ions has to be determined for each cycle. Figure 7(b) illustrates the counting rate of PMT $n_{\rm photon}$ as a reference for the relative luminosity. These counts originate mainly from the beam-target interactions. The background counting rate of the PMT without the gas target was typically less than 10 Hz. Since the counting rate of the PMT $n_{\rm photon}$ also varies from cycle to cycle, the luminosity has to be determined for each cycle. The ratio of $n_{\rm photon}/n_{\rm ion}$ is also shown in Fig. 7(c) for monitoring the effective thickness of internal target. In most of the cycles the ratios appear to vary a little. This demonstrates that the effective target thickness also varies a little during the experiment run.

As a consequence, the effective target thickness and mean ion current, hence the luminosity, have to be determined for each cycle. The counting rate of the PMT can be used as a relative measure of the luminosity over the whole experiment run, and was calibrated by beam current and effective target thickness which was determined from the beam energy losses. The values of the luminosity obtained during the experiment ranged between 3.8×10^{24} and 2.6×10^{25} $\rm cm^{-2}s^{-1}$. A total integrated luminosity of 1.15×10^{30} $\rm cm^{-2}$ in about 22 hours was determined. As an independent check on the energy-loss method, we have measured X-rays produced from the K-REC process with a known angle differential cross section [14, 15]. The integrated luminosity here is given by

$$L = n_{\rm X}\left(\frac{{\rm d}\sigma}{{\rm d}\Omega}\right)^{-1}(\Delta\Omega)^{-1}, \tag{5}$$

where $n_{\rm X}$ is the produced X-ray yield from the K-REC process, ${\rm d}\sigma/{\rm d}\Omega$ the angular differential cross section, and $\Delta\Omega$ the solid angle of the detector. The integrated luminosities of 1.12×10^{30} and 1.09×10^{30} $\rm cm^{-2}$ were determined by two lead-shielded HPGe detectors which were oriented at 90° and 120° with respect to the beam path, respectively. The main errors for luminosity measurement with HPGe come from intrinsic efficiencies and solid angles of detectors. Here intrinsic efficiencies were calibrated through standard radioactive sources. The errors of solid angles are caused mainly by non-ideal collisions of beam and target. The errors of the two are 3.0% and 3.4%, respectively, and the total error is estimated to be about 5%.

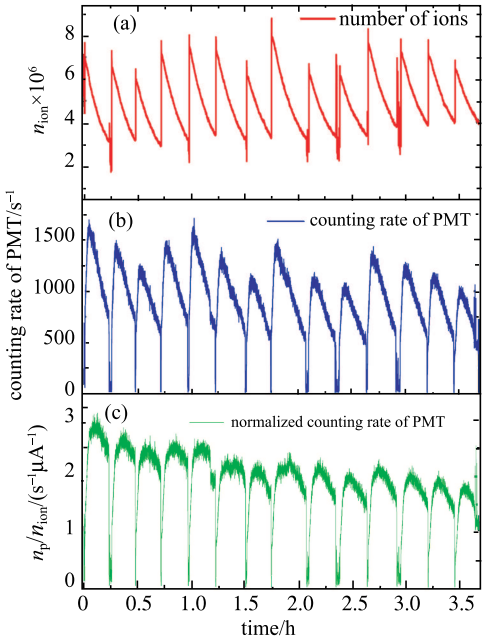

Fig. 7. (color online) (a) The number of Xe^{54+} ion $n_{\rm ion}$ in CSRe, (b) the counting rate of PMT $n_{\rm photon}$, and (c) the ratio of $n_{\rm photon}/n_{\rm ion}$ for a sample of machine cycles. The data shown in (b) and (c) here represented the relative luminosity and thickness as a function of time, respectively.

Since the measurement of the beam current with the DCCT is accurate to 1%—3%, the rate of the revolution-frequency shift can be accurate to about 2%, and the counting rate of the PMT is accurate to about 3%, so the total uncertainty in the determination of the luminosity via the beam-energy-loss method in our case is about 5%.

4 Conclusions

The effective target thickness for nitrogen has been determined from the energy losses of 197 MeV/u Xe^{54+} ion beams in HIRFL-CSRe. A value of $(2.21\pm0.11)\times10^{12}$ atoms/cm^2 for nitrogen was determined at the beginning of the measurement and then decreased to $(9.06\pm0.45)\times10^{11}$ atoms/cm^2. The measured thicknesses were compared to the corresponding value estimated by the pressure difference measurements, which were calibrated by the flow rate of atomic beam. Possible sources of discrepancy arising from the influence of beam-target overlaps in the ring were analysed. An corresponding integrated luminosity of $(1.15 \pm 0.06) \times 10^{30}$ cm^{-2} was also determined in this way. As an independent check on the energy-loss method, we have also measured the produced X-ray yields from the K-REC processes with a known angle differential cross section. The integrated luminosities of $(1.12\pm0.06)\times10^{30}$ and $(1.09\pm0.06)\times10^{30}$ cm^{-2} were determined by two HPGe detectors which were oriented at 90° and 120°, respectively. The consistent results show that the the energy-loss technique can be used to measure the effective target thickness and luminosity in future experiments at the HIRFL-CSRe internal target.

We would like to thank the crew of Accelerator Department for their skillful operation of the HIRFL-CSR accelerator complex.

References

1 C. Ekström, Nucl. Instrum, Methods A, **362**: 1–15 (1995)
2 C. Ekström, Nucl. Phys. A, **626**: 405–416 (1997)
3 J. W. Xia, W. L. Zhan, B. W. Wei et al, Nucl. Instrum, Methods A, **488**: 11–25 (2002)
4 Y. J. Yuan, J. C. Yang, J. W. Xia et al, Nucl. Instrum, Methods B, **317**: 214–217 (2013)
5 X. Cai, R. Lu, C. Shao et al, Nucl. Instrum, Methods A, **555**: 15–19 (2005)
6 Xiao-Hong Cai, Cao-Jie Shao, Rong-Chun Lu et al, Chin. Phys. C, **31** (8): 750–754 (2005)
7 R. C. Lu, *Construction of HIRFL-CSRe Cluster Internal Target*, M.S. Thesis (Lanzhou: Insititute of Morden Physics, CAS, 2005) (in Chinese)
8 Yongdong Zang, Ruishi Mao, Junxia Wu et al, High Power Laser and Particle Beams, **23** (7): 1899–1903 (2011) (in Chinese)
9 A. Täschner, E. Köhler, H.W. Ortjohann et al, Nucl. Instrum, Methods A, **660**: 22–30 (2010)
10 H. J. Stein, M. Hartmann, I. Keshelashvili et al, Phys. Rev. ST Accel. Beams, **11**: 052801 (2008)
11 Xiao-Dong Yang, Li-Jun Mao, Guo-Hong Li et al, Chin. Phys. C, **34** (07): 998–1004 (2010)
12 U. Schramm, D. Habs, Progress in Particle and Nuclear Physics, **53**: 583–677 (2004)
13 B. A. Weaver, A. J. Westphal, Nucl. Instrum, Methods B, **187**: 285–301 (2002)
14 D. Yu, Y. Xue, C. Shao et al, Nucl. Instrum, Methods B, **269**: 692–694 (2011)
15 T. Ludziejewski, Th. Stöhlker, D. C. Ionescu et al, Phys. Rev. A, **61**: 052706 (2000)